Structure-Based Drug Design of Novel, Potent, and Selective Azabenzimidazoles (ABI) as ATR Inhibitors
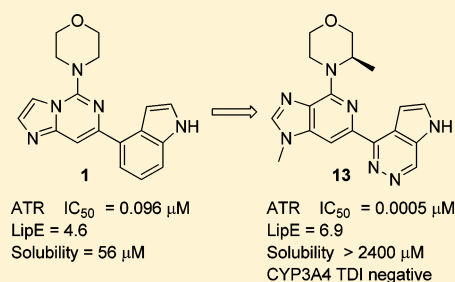
Paul A Barsanti,*,[†] Yue Pan, Yipin Lu, Rama Jain, Matthew Cox, Robert J. Aversa, Michael P. Dillon, Robert Elling, Cheng Hu, Xianming Jin, Mark Knapp, Jiong Lan, Savithri Ramurthy, Patrick Rudewicz, Lina Setti, Sharadha Subramanian, Michelle Mathur, Lorena Taricani, George Thomas, Linda Xiao, and Qin Yue

Global Discovery Chemistry/Oncology, Novartis Institutes for Biomedical Research, 5300 Chiron Way, Emeryville, California 94608, United States

S Supporting Information

ABSTRACT: Compound **13** was discovered through morphing of the ATR biochemical HTS hit **1**. The ABI series was potent and selective for ATR. Incorporation of a 6-azaindole afforded a marked increase in cellular potency but was associated with poor PK and hERG ion channel inhibition. DMPK experiments established that CYP P450 and AO metabolism in conjunction with Pgp and BCRP efflux were major causative mechanisms for the observed PK. The series also harbored the CYP3A4 TDI liability driven by the presence of both a morpholine and an indole moiety. Incorporation of an adjacent fluorine or nitrogen into the 6-azaindole addressed many of the various medicinal chemistry issues encountered.

1
ATR IC_{50} = 0.096 μM
LipE = 4.6
Solubility = 56 μM

13
ATR IC_{50} = 0.0005 μM
LipE = 6.9
Solubility > 2400 μM
CYP3A4 TDI negative

KEYWORDS: ATR, structure-based drug design, CYP3A4 TDI, aldehyde oxidase

Complex networks of cellular surveillance mechanisms maintain genomic integrity in the face of various genomic insults. Ataxia telangiectasia and Rad-3 related protein (ATR) regulates the S and G2 checkpoints along with DNA repair following exposure to DNA damaging agents which interfere with DNA replication.[1] Recently, several reports have demonstrated the sensitization of cancer cells to cytotoxic agents when combined with ATR inhibitors,[2,3] potentially providing an avenue to explore the possibility of developing a selective ATR inhibitor for use as a chemosensitizer. However, sustained inhibition of ATR alone can potentially lead to cell death in tumor cells as a direct consequence of inducing DNA damage selectively in the S phase. From a hypothesis-driven siRNA screen, in the presence of a potent and selective low molecular weight ATR inhibitor, we identified ATM (Ataxia telangiectasia mutated) deficiency to be synthetically lethal with ATR inhibition, thus providing a potential genetic stratification for therapeutic ATR inhibition as a monotherapy. We describe herein the discovery of novel, potent, and highly selective azabenzimidazoles as ATR inhibitors, which were morphed from an initial HTS hit.

Our cellular HTS campaign was developed based on the initial findings in our Developmental and Molecular Pathways group, which identified ATR as a target that synergized with cisplatin when it was inhibited in p53 null cancer cell lines. The cellular screening efforts yielded numerous chemotypes as potential starting points to begin our medicinal chemistry program. However, as we began to profile our HTS hits in our internal kinase selectivity panel consisting of over 60 different kinases, it became very apparent that many of the chemotypes inhibited numerous other kinases. In particular, the vast majority of our cellular hits inhibited most of our lipid kinase panel. For instance, analysis of our selectivity data showed 70% of our ATR hits inhibited PI3Kδ and PI3Kγ (IC_{50} < 1 μM), while almost 50% of the hits inhibited PI3Kα (IC_{50} < 1 μM). In addition, most of the hits also inhibited PI3Kβ, PI4Kβ, mTOR, and VPS34 to varying degrees. Given this selectivity challenge presented by the output of our cellular HTS, we wondered if there were other more selective starting points that might have been missed due to being below some nominal amount of ATR potency to allow detection in a cellular assay or suboptimal physicochemical properties leading to poor cell permeability.

To this end, we utilized a combination of virtual screening along with running a 7% "diverse slice" of the Novartis compound archive. This afforded multiple new chemotypes that had not been realized in the cellular HTS campaign. Most importantly, unlike the cellular HTS efforts, the highly focused and miniaturized pilot biochemical HTS efforts successfully identified several chemotypes that exhibited great improvements in lipid kinase selectivity. One of the initial hits was the highly selective morpholino-imidazopyrimidine **1** (Figure 1). When run through our internal kinase panel, we were amazed to find it did not have any inhibitory activity on any of the 76
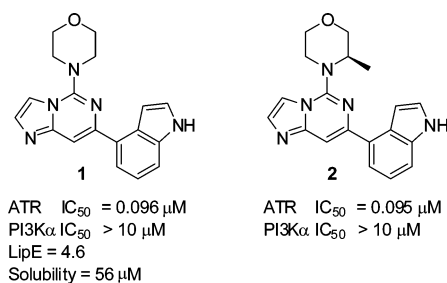
Figure 1. Initial HTS hit **1** and analogue **2**.

kinases tested ($IC_{50} > 8 \mu M$). With an ATR biochemical IC_{50} of 96 nM and a lipophilic efficiency (LipE) of 4.6, despite the presence of an indole, compound **1** was deemed a very favorable starting point.

Compound **1** was modeled into the ATR homology model built based on the PI3Kδ X-ray structure (Figure 2). The
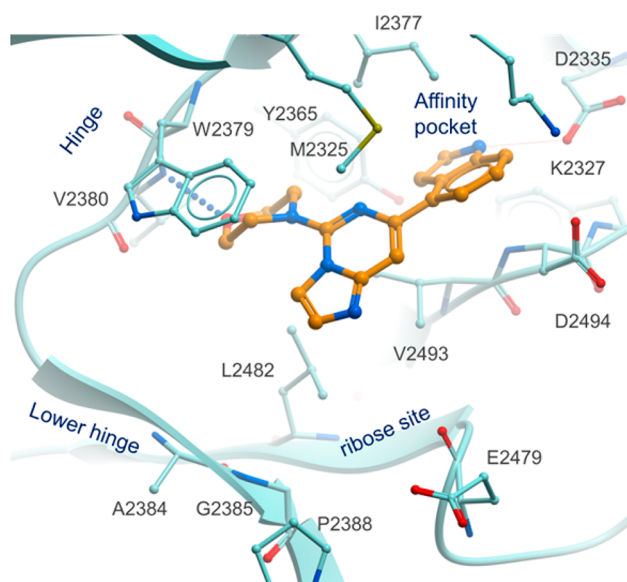

Figure 2. Binding model of compound **1** built based on ATR homology model.

binding model suggested that compound **1** binds to the ATP site with the morpholine ring as the hinge binder, which forms a hydrogen bond with the backbone NH of V2380. The indole group adopts a conformation with about a 30° torsional angle relative to the imidazopyrimidine core and fits nicely in the buried "affinity pocket". The indole ring is sandwiched between the D2494 backbone and I2377 side chain, with the indole NH likely forming a hydrogen bond with D2335, either directly or mediated by a water molecule. Although most of the residues in the affinity pocket are highly conserved in ATR compared to the PI3Ks and other PI3K-related kinases (PIKKs), subtle differences between their sequences and 3D conformations due to nonconserved second shell residues may lead to selectivity. For example, unlike most of the other kinases that have a conserved DFG motif, ATR has a DFN (D2494F2495N2496), which could possibly change the conformational flexibility and preference of the protein.

It soon became apparent that the series represented by **1** may not have the optimal vectors to target key residues and improve potency in the adenine site and the ribose site. Because of the proximity between the morpholine CH_2 adjacent to the N and

the methine of the core, the morpholine is likely twisted relative to the imidazopyrimidine core and therefore does not have the optimal trajectory to explore a small hydrophobic site near M2325 to improve potency. This could explain the lack of increased ATR binding affinity on the addition of a methyl group as in compound **2**. The structure−activity relationship (SAR) at the C-2 position of the core was also somewhat flat (data not shown) since we were limited to targeting residues in the lower hinge, such as with compound **3** (Figure 3). To this end, we redesigned the core by simply moving the bridge nitrogen one atom over thus giving an azabenzimidazole (ABI) core.
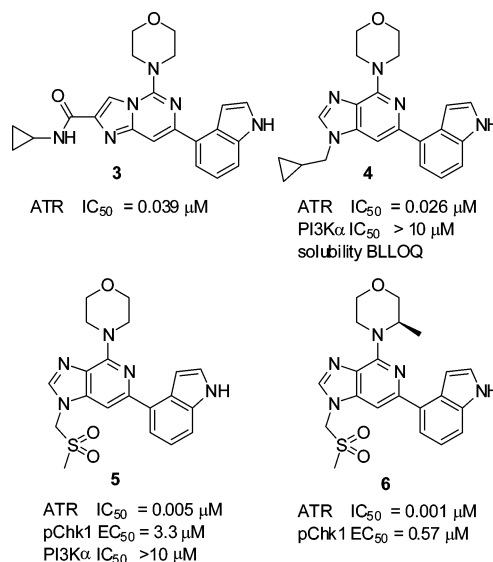

Figure 3. Morphing imidazopyrimidine HTS series into the ABI lead series.

Unlike compound **1**, the N-1 position in the azabenzimidazole core now has the correct valence to allow for substitution down toward a pocket created by G2385, L2482, A2384, P2388, and E2479 in the ribose pocket. On the basis of the in-house ATR homology model, we proposed a cyclopropylmethyl group (**4**) should fit nicely in this small pocket and improve potency through extensive VDW contacts, as can be seen in Figure 4. While the addition of the cyclopropylmethyl improved ATR binding affinity, with a logD of 3.8, the increase in lipophilicity negatively impacted the physicochemical properties, which manifested themselves as poor solubility (below the lower limit of quantification, BLLOQ) and low microsomal stability (mouse = 75, rat = 37, human = 12 mL/min/kg). To address the high lipophilicity, we increased the polarity by switching to a sulfone, leading to compound **5** (Figure 3). We were pleased to find that compound **5** exhibited good solubility, permeability, and microsomal stability, which translated *in vivo* leading to a low clearance compound with excellent oral bioavailability in the rat (Table 1).

Since repositioning the core nitrogen in **1** to the ABI relieved the torsional strain between the core and the morpholine, the morpholine now has the correct trajectory to approach the M2325 pocket. As a result, the *R*-methyl morpholine in **6** brings about a 5-fold increase in ATR binding affinity compared to **5**. For the first time cellular target modulation activity (as judged by pChk1 inhibition) was observed at less than 1 μM. As we continued to improve potency, the homology model
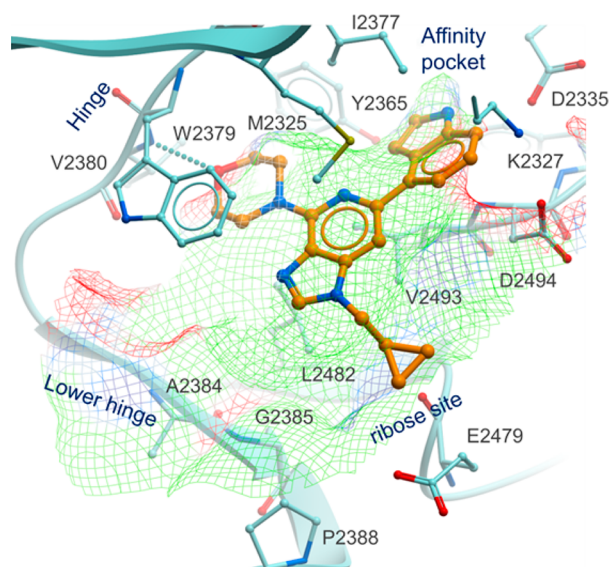
Figure 4. Binding model of compound **4** built based on ATR homology model. The ligand accessible surface is shown by the colored mesh. The methyl cyclopropyl in **4** makes productive VDW contacts in the ribose site.

Table 1. Property Data for Compound 5

solubility $(\mu M)^a$	Caco-2 A-B/B-A^b	Cl_{int} M/R/H^c	rat Cl $(mL/min/kg)^d$	rat % F^d
193	14/58	31/30/6	14	96

^{a}Measured using miniaturized shake flask equilibrium solubility assay with PBS buffer at pH 7.0. $^b P_{app}$ ($\times 10^{-6}$ cm/s), pH 7.4, 10 μM compound concentration. ^{c}Mouse/rat/human microsomal intrinsic clearance scaled to hepatic blood flow. ^{d}Administered 2.5 mg/kg i.v. and 5.0 mg/kg p.o. to RT-Sprague–Dawley male rats.

suggested the possibility of picking up an additional hydrogen bond to K2327 in the affinity pocket. Incorporation of a 6-nitrogen into the indole, together with the addition of a methyl group to the methylene carbon between the ABI core and the sulfone, led to the highly potent and soluble compound **7** (Figure 5, stereocenter next to the sulfone was arbitrarily
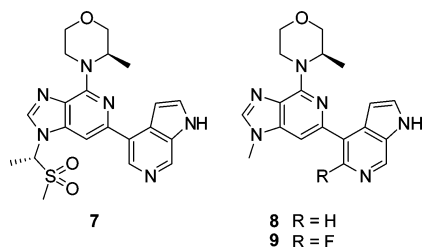

Figure 5. 6-Azaindole analogues.

assigned as *R*, see Supporting Information). When we followed up with additional selectivity assays, we were pleased to find **7** exhibited a remarkable selectivity profile. Apart from not inhibiting the closely related ATM (2 μM) and DNAPK (10 μM) kinases, it also did not inhibit any of the PI3Kα, β, γ, or δ kinases below 8 μM. Additionally, **7** did not have any inhibitory activity under 10 μM in over 60 of our internal enzymatic kinase assays. However, while **7** had a very desirable *in vitro* biological profile (highly selective, potent in cells, and highly soluble), as can be seen from the data in Table 2, **7** had a poor

in vivo profile in addition to several potential safety issues. While the intrinsic clearance in rat microsomes was moderate (34 mL/min/kg), compound **7** had extremely high *in vivo* clearance in rat (114 mL/min/kg) and no oral bioavailability. The Caco-2 data showed low permeability and substantial efflux, which also contributed to the poor bioavailability. Furthermore, **7** inhibited the hERG ion channel, and while it showed no reversible inhibition of any of the four major cytochrome P450 isoforms (3A4, 2D6, 2C9, and 1A2, all >40 μM), it was positive when tested for time-dependent inhibition (TDI) of CYP 3A4.

Our SAR at this time suggested the polar sulfone and the 6-nitrogen in the azaindole were the recognition elements for the Pgp pump that was driving the efflux observed in the Caco-2 assay. In the hope of improving the permeability we truncated the polar sulfone group to a methyl group, thus reducing the polar surface area. We were pleased to find compound **8** maintained ATR biochemical potency (0.4 nM) and increased the permeability ($P_{app} = 6 \times 10^{-6}$ cm/s). Unfortunately, this resulted in only modest improvements in the rat PK ($V_{ss} = 2.3$ L/kg, Cl = 49 mL/min/kg, and $F = 18\%$). Since both **7** and **8** exhibited high *in vivo* clearance and poor *in vitro/in vivo* correlation (IVIVC) with respect to the moderate rat microsomal intrinsic clearance, we suspected other clearance mechanisms might be operative, in addition to CYP-mediated metabolism. Suspecting biliary excretion as a possible explanation, we tested **8** in a small panel of ABC transporters (MDR1, MRP2, and BCRP) and found it was a substrate for BCRP ($V_{max} = 130$ nmol/mg/min and $K_m = 2.0$ μM) and MDR1 ($V_{max} = 140$ nmol/mg/min and $K_m = 108$ μM) efflux transporters. Furthermore, metabolism identification (MetID) experiments that employed ^{18}O-labeled water in cytosolic incubations revealed the involvement of aldehyde oxidase (AO) in the metabolism of **8**.^{4,5} In addition, from a safety perspective, **8** still possessed hERG and CYP3A4 TDI liabilities. While the high *in vivo* clearance of **8** was complex and multifactorial, it was apparent from our SAR that the higher pK_a of the 6-nitrogen in the azaindole brought along many issues since **5** had excellent PK (Table 1) and no hERG channel inhibition liability (hERG IC$_{50}$ > 30 μM, dofetilide binding assay). To this end we focused our attention on modifications to the azaindole. These efforts resulted in the highly potent compound **9** (Figure 5) where installation of a 5-fluoro on the 6-azaindole simultaneously eliminated Pgp (as judged by B-A/A-B in the Caco-2 assay) and BCRP efflux, as well as shut down AO metabolism, leading to good rat PK ($V_{ss} = 1.2$ L/kg, Cl = 20 mL/min/kg, and $F = 66\%$). Additionally, the 5-fluoro dialed out the hERG inhibition signal. However, it did not eliminate the CYP3A4 TDI liability. Given that CYP3A4 is the most common metabolizing enzyme involved in the metabolism of many drug molecules, we were concerned with the potential for clinically relevant drug−drug interaction (DDI) if **9** was coadministered with a drug whose metabolism was dependent on CYP3A4. In order to gain understanding of the mechanism(s) causing the TDI, we ran MetID experiments that utilized microsomal incubations in the presence of various trapping agents in order to pinpoint the site of metabolism. We were surprised to find that the MetID experiments were unable to detect either GSH or cyanide adducts. This may simply be due to the inability of the reactive metabolite to diffuse away from CYP3A4's active site and be trapped with exogenous nucleophiles, and is not *per se* indicative that reactive metabolites were not being formed. From the structural alert

Table 2. Property Data for Compounds 7−9

compd	ATR IC$_{50}$ (μM)	pChk1 IC$_{50}$ (μM)[a]	mTOR cell IC$_{50}$ (μM)[b]	solubility (μM)[c]	Caco-2 A-B/B-A[d]	hERG IC$_{50}$ (μM)[e]	rat Cl$_{int}$ (mL/min/kg)[f]	rat %F[g]	CYP3A4 TDI[h]
7	0.0002	0.080	>4.6	>770	2/37	9	34	0	positive
8	0.0004	0.084	7.5	>1700	6/44	13	33	18	positive
9	0.0001	0.096	n.d.	>2300	38/38	>30	33	66	positive

[a]Inhibition of pChk1 Ser345 in HeLa S3 cells exposed to 1 μM gemcitabine and test compound for 4 h. [b]Subconfluent TSC1 −/− MEF cells were harvested by trypsinization and cultured overnight at 37 °C. Test compounds were added to the cells for 1 h at 37 °C, 5% CO$_2$. Samples were further processed using the AlphaScreen SureFire p70 S6K (p-Thr389) Assay Kit. [c]Measured using miniaturized shake flask equilibrium solubility assay with PBS buffer at pH 7.0. [d]P_{app} ($\times 10^{-6}$ cm/s), pH 7.4, 10 μM compound concentration. [e]hERG ^{3}H-dofetilide binding assay. [f]Rat microsomal intrinsic clearance scaled to hepatic blood flow. [g]Administered 2.5 mg/kg i.v. and 5.0 mg/kg p.o. to RT-Sprague−Dawley male rats. [h]Test compound (50 μM with serial dilutions) is incubated with human liver microsome (0.5 mg/mL) in phosphate buffer (100 mM) with NADPH (1 mM) for 0, 5, 15, and 30 min. The incubation mixture is then diluted 20 times and incubated with CYP3A4 substrate midazolam (20 μM) to determine residual CYP3A4 enzyme activity. The enzyme activity vs incubation time is plotted to obtain kinetic parameters for TDI.

perspective, the ABI series contained both a cyclic amine and an indole, two well documented TDI liabilities.[6,7] The six-membered morpholine ring had the potential to generate a reactive iminium ion through oxidation on the α-carbon, while the indole had the possibility of forming a reactive epoxide between C2 and C3. To this end, we made the bridged morpholine 10, which is incapable of forming the iminium ion due to ring strain. As can be seen in Figure 6, compound 10

10
ATR   IC$_{50}$ = 0.034 μM
TDI k$_{inact}$ / K$_I$ = 0.002 uL/min/pmol

11
ATR   IC$_{50}$ = 0.006 μM
TDI k$_{inact}$ / K$_I$ = 0.002 uL/min/pmol

12
ATR   IC$_{50}$ = 0.19 μM
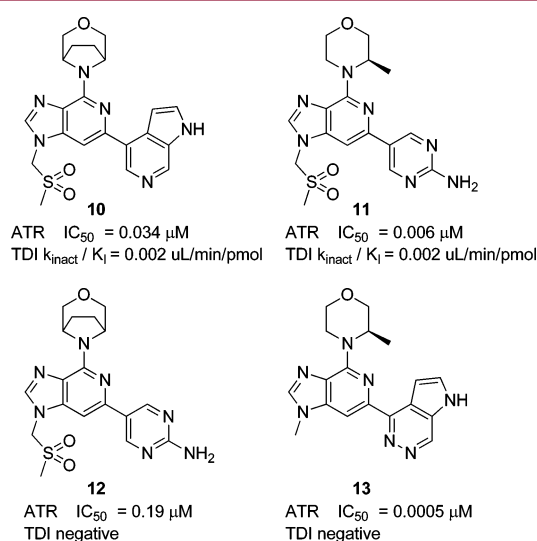TDI negative

13
ATR   IC$_{50}$ = 0.0005 μM
TDI negative

Figure 6. CYP3A4 TDI SAR.

was still TDI positive. Interestingly, when we removed the azaindole in 9 and replaced it with other moieties that are not known CYP TDI liabilities such as the aminopyrimidine in 11, the compound was also TDI positive. It was not until both the methyl morpholine and the azaindole were simultaneously removed (compound 12) that the compound was devoid of

TDI activity, indicating that both the methyl morpholine and the azaindole contribute to the TDI.

The need to maintain both ATR activity and kinase selectivity left few options for azaindole and morpholine replacements as the SAR was very steep in these regions. Building on our SAR that led to 9, we focused on other electronic perturbations to the azaindole. We found that incorporating 1H-pyrrolo[2,3-d]pyridazine into compounds such as 13 (Figure 6) had the desired effects of removing the hERG liability and being consistently devoid of CYP3A4 TDI. The lower pK_a and the extra nitrogen likely disrupted hERG and CYP 3A4 binding. Importantly, compound 13 also effectively maintained ATR potency (0.5 nM) and other key attributes related to selectivity and reversible CYP P450 inhibition (Table 3). Furthermore, in line with our findings of ATM deficiency being synthetically lethal with ATR inhibition, compound 13 was effective at inhibiting the growth of the ATM null HT144 human melanoma cell line with a GI$_{50}$ of 0.35 μM. The potency shift from the biochemical assay to the cellular assay was consistent with the high cellular ATP concentration. Compound 13 was studied in rat PK (2.5 mg/kg i.v. and p.o.), and although the bioavailability was low (7.5%), the clearance was moderate (34 mL/min/kg, although still higher than the predicted value of 11 mL/min/kg from microsome) with the V_{ss} at 1.8 L/kg and $t_{1/2}$ at 2 h. The low bioavailability is likely the result of low permeability and efflux.

The synthesis of compound 13 is shown in Scheme 1. Reduction of the nitro group followed by ring cyclization gave the ABI core 15. A SNAr reaction with (R)-3-methylmorpholine provided 16, which underwent methylation to provide 17. Compound 17 was then converted to the boronic ester and subjected to a Suzuki coupling reaction to give 18 in good yields. Final deprotection of the tosyl group afforded 13.

In conclusion, compound 13 was discovered through morphing the core of an ATR biochemical screening hit. Incorporation of a 6-azaindole afforded a marked increase in cellular potency but was associated with poor PK and hERG

Table 3. Property Data for Compound 13

ATR IC$_{50}$ (μM)	ATM IC$_{50}$ (μM)	DNAPK IC$_{50}$ (μM)	mTOR cell IC$_{50}$ (μM)[a]	HT144 GI$_{50}$ (μM)[b]	solubility (μM)[c]	hERG IC$_{50}$ (μM)[d]	CYP IC$_{50}$ (μM)[e]	Caco-2 A-B/B-A[f]
0.0005	15	>25	>13	0.35	>2400	>30	all >24	3.6/38

[a]Subconfluent TSC1 −/− MEF cells were harvested by trypsinization and cultured overnight at 37 °C, 5% CO$_2$. Test compounds were added to the cells for 1 h at 37 °C, 5% CO$_2$. Samples were further processed using the AlphaScreen SureFire p70 S6K (p-Thr389) Assay Kit. [b]Cell Titer Glow assay with 72 h continuous exposure to compound 13. [c]Measured using miniaturized shake flask equilibrium solubility assay with PBS buffer at pH 7.0. [d]Determined using automated whole cell electrophysiology. [e]Cytochrome P450 isoforms 3A4, 2D6, 2C9, and 1A2. [f]P_{app} ($\times 10^{-6}$ cm/s), pH 7.4, 10 μM compound concentration.

Scheme 1[a]
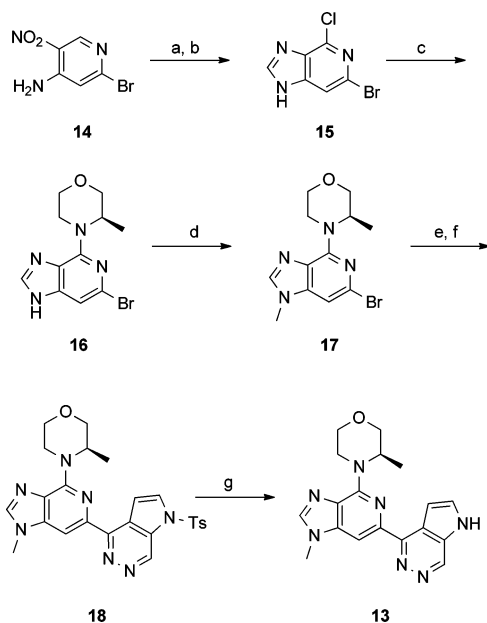
[a]Reagents and conditions: (a) SnCl$_2$·2H$_2$O, conc. HCl, 90 °C, 89%; (b) CH(OEt)$_3$, Ac$_2$O, 90 °C, then NaOH, 55 °C, 100%; (c) (R)-3-methylmorpholine, TEA, 140 °C, 66%; (d) MeI, K$_2$CO$_3$, NMP, 80 °C, 95%; (e) Bis(pinacolato)diboron, PdCl$_2$(dppf)·CH$_2$Cl$_2$ adduct, KOAc, dioxane, 90 °C; (f) 4-chloro-1-tosyl-1H-pyrrolo[2,3-d]pyridazine, Na$_2$CO$_3$, bis(tri-tert-butylphosphine)palladium, DME, H$_2$O, 35%; (g) NaOH, H$_2$O, MeOH, 55 °C, 65%.

ion channel inhibition. DMPK experiments established that CYP p450 and AO metabolism in conjunction with Pgp and BCRP efflux were the major underlying mechanisms. Incorporation of an adjacent fluorine to the 6-azaindole eliminated AO metabolism and efflux issues, affording compounds with good oral exposure and devoid of hERG inhibition. Despite this breakthrough the ABI series still suffered from a CYP3A4 TDI liability, driven by the presence of both a morpholine and indole moiety. This was remedied by installation of an additional nitrogen into the 6-azaindole ring leading to the potent, selective, soluble, hERG, and TDI negative compound 13, which also exhibited a reasonable i.v. PK profile. Compound 13 represents a candidate that can be further profiled to help validate our hypothesis on the synthetic lethality relationship between ATM deficiency and ATR inhibition *in vivo*.

■ ASSOCIATED CONTENT

Ⓢ Supporting Information
Synthetic procedures, characterization data, and assay information. This material is available free of charge via the Internet at http://pubs.acs.org.

■ AUTHOR INFORMATION

Corresponding Author
*E-mail: pbarsanti@nurix-inc.com.

Present Address
†Nurix, Inc., 1700 Owens Street, Suite 290, San Francisco, California 94158, United States.

Notes
The authors declare no competing financial interest.

■ REFERENCES
(1) Weinert, T. A. DNA damage checkpoint meets the cell cycle engine. *Science* **1997**, *277*, 1450−1451.

(2) Foote, K. M.; Blades, K.; Cronin, A.; Fillery, S.; Guichard, S. S.; Hassall, L.; Hickson, I.; Jacq, X.; Jewsbury, P. J.; McGuire, T. M.; Nissink, J. W. M.; Odedra, R.; Page, K.; Perkins, P.; Suleman, A.; Tam, K.; Thommes, P.; Broadhurst, R.; Wood, C. Discovery of 4-{4-[(3R)-3-methylmorpholin-4-yl]-6-[1-(methylsulfonyl)cyclopropyl]pyrimidin-2-yl}-1H-indole (AZ20): a potent and selective inhibitor of ATR protein kinase with monotherapy in vivo antitumor activity. *J. Med. Chem.* **2013**, *56*, 2125−2138.

(3) Charrier, J. D.; Durrant, S. J.; Golec, J. M. C.; Kay, D. P.; Knegtel, R. M. A.; MacCormick, S.; Mortimore, M.; O'Donnell, M. E.; Pinder, J. L.; Reaper, P. M.; Rutherford, A. P.; Wang, P. S. H.; Young, S. C.; Pollard, J. R. Discovery of potent and selective inhibitors of ataxia telangiectasia mutated and Rad3 related (ATR) protein kinase as potential anticancer agents. *J. Med. Chem.* **2011**, *54*, 2320−2330.

(4) Garattini, E.; Terao, M. The role of aldehyde oxidase in drug metabolism. *Expert Opin. Drug Metab. Toxicol.* **2012**, *8*, 487−503.

(5) Morrison, R. D.; Blobaum, A. L.; Byers, F. W.; Santomango, T. S.; Bridges, T. M.; Stec, D.; Brewer, K. A.; Sanchez-Ponce, R.; Corlew, M. M.; Rush, R.; Felts, A. S.; Manka, J.; Bates, B. S.; Venable, D. F.; Rodriguez, A. L.; Jones, C. K.; Niswender, C. M.; Conn, P. J.; Lindsley, C. W.; Emmitte, K. A.; Daniels, J. S. The role of aldehyde oxidase and xanthine oxidase in the biotransformation of a novel negative allosteric modulator of metabotropic glutamate receptor subtype 5. *Drug Metab. Dispos.* **2012**, *40*, 1834−1845.

(6) Hollenberg, P. F.; Kent, U. M.; Bumpus, N. N. Mechanism-based inactivation of human cytochromes P450s: experimental character-ization, reactive intermediates, and clinical implications. *Chem. Res. Toxicol.* **2008**, *21*, 189−205.

(7) Safina, B. S.; Baker, S.; Baumgardner, M.; Blaney, P. M.; Chan, B. K.; Chen, Y.; Cartwright, M. W.; Castanedo, G.; Chabot, C.; Cheguillaume, A. J.; Goldsmith, P.; Goldstein, D. M.; Goyal, B.; Hancox, T.; Handa, R. K.; Iyer, P. S.; Kaur, J.; Kondru, R.; Kenny, J. R.; Krintel, S. L.; Li, J.; Lesnick, J.; Lucas, M. C.; Lewis, C.; Mukadam, S.; Murray, J.; Nadin, A. J.; Nonomiya, J.; Padilla, F.; Palmer, W. S.; Pang, J.; Pegg, N.; Price, S.; Reif, K.; Salphati, L.; Savy, P. A.; Seward, E. M.; Shuttleworth, S.; Sohal, S.; Sweeney, Z. K.; Tay, S.; Tivitmahaisoon, P.; Waszkowycz, B.; Wei, B.; Yue, Q.; Zhang, C.; Sutherin, D. P. Discovery of novel PI3-kinase δ specific inhibitors for the treatment of rheumatoid arthritis: taming CYP3A4 time-dependent inhibition. *J. Med. Chem.* **2012**, *55*, 5887−5900.